

# Effect of ground motion processing and filtering on the response of rocking structures

**Journal Article****Author(s):**

Elmorsy, Medhat; Vassiliou, Michalis F.

**Publication date:**

2023-05

**Permanent link:**

<https://doi.org/10.3929/ethz-b-000601584>

**Rights / license:**

[Creative Commons Attribution-NonCommercial 4.0 International](#)



**Originally published in:**

Earthquake Engineering & Structural Dynamics 52(6), <https://doi.org/10.1002/eqe.3837>

**Funding acknowledgement:**

ETH-11 21-1 - Physical modelling of reinforced concrete structures using 3D printing (ETHZ)

# Effect of ground motion processing and filtering on the response of rocking structures

Medhat Elmorsy<sup>1,2</sup>  | Michalis F. Vassiliou<sup>1</sup> 

<sup>1</sup>Chair of Seismic Design and Analysis, Institute of Structural Engineering (IBK), ETH Zürich, Zurich, Switzerland

<sup>2</sup>Structural Engineering Department, Mansoura University, Mansoura, Egypt

## Correspondence

Michalis F. Vassiliou, IBK, ETH Zurich, Stefano Francini Platz 5, CH-8097 Zurich, Switzerland.

Email: [vassiliou@ibk.baug.ethz.ch](mailto:vassiliou@ibk.baug.ethz.ch)

## Funding information

Eidgenössische Technische Hochschule Zürich

## Abstract

With growing interest in rocking structures, it is important to quantify the effects of ground motion processing schemes on rocking response. To this end, this paper studied the influence of different ground motion correction schemes and parameter values on the rocking displacement spectrum. When the problem is treated on an individual ground motion basis, then it seems that ground motion correction *does* have an influence on the rocking response, especially for more slender blocks. This influence is larger for causal filtering. However, no specific trend related to the cut off period of the filter can be observed (at least for cut off periods longer than or equal to 10 s) or on the type of the recording device (analog or digital). On the other hand, when treating the problem statistically (by comparing the statistics of the response due to sets of ground motion, not a single ground motion), the effect is significantly reduced: The processing schemes do not induce any significant bias to the rocking response and the motion-to-motion variability seems more important than the ground motion correction method. This conclusion applies to both analog and digital records, both causal and acausal filters, and to all near field pulse like, near field no pulse like, and far field records.

## KEYWORDS

analog ground motion records, digital filtering, digital ground motion records, ground motion processing, rocking, uplifting structures

## 1 | INTRODUCTION

The use of recorded ground motions is a cornerstone of contemporary earthquake engineering, as it allows for the quantification of seismic action. Recording of ground motions typically involves measurements of the ground acceleration that are integrated to obtain velocity and displacement traces. Velocity traces should show zero values at the end of the record and displacement traces should reflect the residual displacement (often referred to as the fling step) at the recording site, acquired from geodetic data. However, this is not the case because recorded motions are unavoidably plagued by different sources of noise<sup>1–4</sup> that result in physically unrealistic velocity or displacement time series.

This is an open access article under the terms of the [Creative Commons Attribution-NonCommercial](https://creativecommons.org/licenses/by-nc/4.0/) License, which permits use, distribution and reproduction in any medium, provided the original work is properly cited and is not used for commercial purposes.

© 2023 The Authors. *Earthquake Engineering & Structural Dynamics* published by John Wiley & Sons Ltd.

**NOVELTY**

- The influence of ground motion correction on the rocking oscillator is studied.
- On a single ground motion basis, ground motion correction influences the response of slender structures.
- On a statistical basis (i.e., by examining the median responses to multiple ground motions) the influence is small.

To enforce a zero velocity at the end and a residual displacement consistent with the geodetic data (if available), ground motions are processed (“corrected”). However, the “true” ground motion cannot be recovered. Several correction procedures have been developed and there is no correction method that can be considered a panacea.<sup>3</sup> Different correction procedures will result in different drawbacks of the corrected trace and the optimal processing scheme depends on the application. The influence of different processing schemes as well as of the values of the parameters of each scheme on elastic and elastoplastic systems has been extensively studied to conclude that it varies according to the period of the elastic system.

However, the notion of structural period is not applicable to the rocking oscillator<sup>5–10</sup>: Unlike the elastoplastic oscillator, there is no “equivalent elastic system” that can be used to predict the response of rocking structures, that is, the linear elastic oscillator cannot be used as a proxy to predict the behavior of a rocking system.<sup>11</sup> The rocking oscillator is worth studying because it can describe a wide range of systems that cannot be adequately described by the elastic oscillator. Examples of such systems are the out of plane motion of masonry structures,<sup>12–21</sup> the motion of unanchored equipment,<sup>22–33</sup> and the response of ancient Greco-Roman and Chinese temples.<sup>34–38</sup> Moreover, allowing a structure to uplift and sustain rocking motion can be used as a seismic design method<sup>39–64</sup> and references therein], because the uplift works as a mechanical fuse and limits the design forces of both the superstructure and the foundation.

This paper focuses on the influence of the processing schemes on the response of rocking structures. After a brief introduction (Section 1), it briefly discusses the rocking oscillator (Section 2) and the sources of noise in accelerograms as well as typical correction procedures (Section 3). Section 4 presents the database of the ground motions that were used, while Section 5 provides a detailed description of the different correction schemes that were examined. Section 6 presents the results in the form of rocking spectra for different correction processes and different values of their parameters.

## 2 | DISPLACEMENT-BASED ANALYSIS OF ROCKING STRUCTURES

Before proceeding with ground motion processing, it is useful to briefly describe the rocking oscillator and underline some of its properties that will facilitate the study of the dependence of its response on ground motion correction methods.

The equation of in-plane motion for a rigid rectangular rocking block (Figure 1A) with slenderness  $\alpha$  and a semi-diagonal  $R$  is:

$$\ddot{\theta} = -p^2 \left( \sin[\pm\alpha - \theta] + \frac{\ddot{u}_g}{g} \cos[\pm\alpha - \theta] \right) \quad (1)$$

where  $p = \sqrt{(3g)/(4R)}$  is the frequency parameter of the rocking column—not to be confused with any sort of natural frequency, as the frequency of free vibration in rocking is amplitude-dependent and ranges from zero to infinity.<sup>5</sup> The upper and the lower sign in front of  $\alpha$  correspond to a positive and a negative tilt angle  $\theta$ , respectively. It is assumed that energy is only dissipated during impact. Housner<sup>5</sup> assumed that (a) the impact is instantaneous and (b) the impact forces are concentrated on the impacting corner. Based on these assumptions, the ratio of post to pre-impact rotational velocities (i.e., the coefficient of restitution) is:

$$r = 1 - \frac{3}{2} \sin^2 \alpha \quad (2)$$

Inspection of Equation (1) shows that the rotational (i.e., tilt angle) response of a rocking block to a given ground motion is a function of two parameters:  $\alpha$  and  $R$ . Similarly, for the elastic oscillator, the response is a function of two parameters: the eigenperiod,  $T$ , and the damping ratio,  $\zeta$ . In elastic structures and for typical values of  $T$  and  $\zeta$ , the dependence on  $T$  is heavier and the concept of the elastic response spectrum has emerged, where the maximum response is plotted against

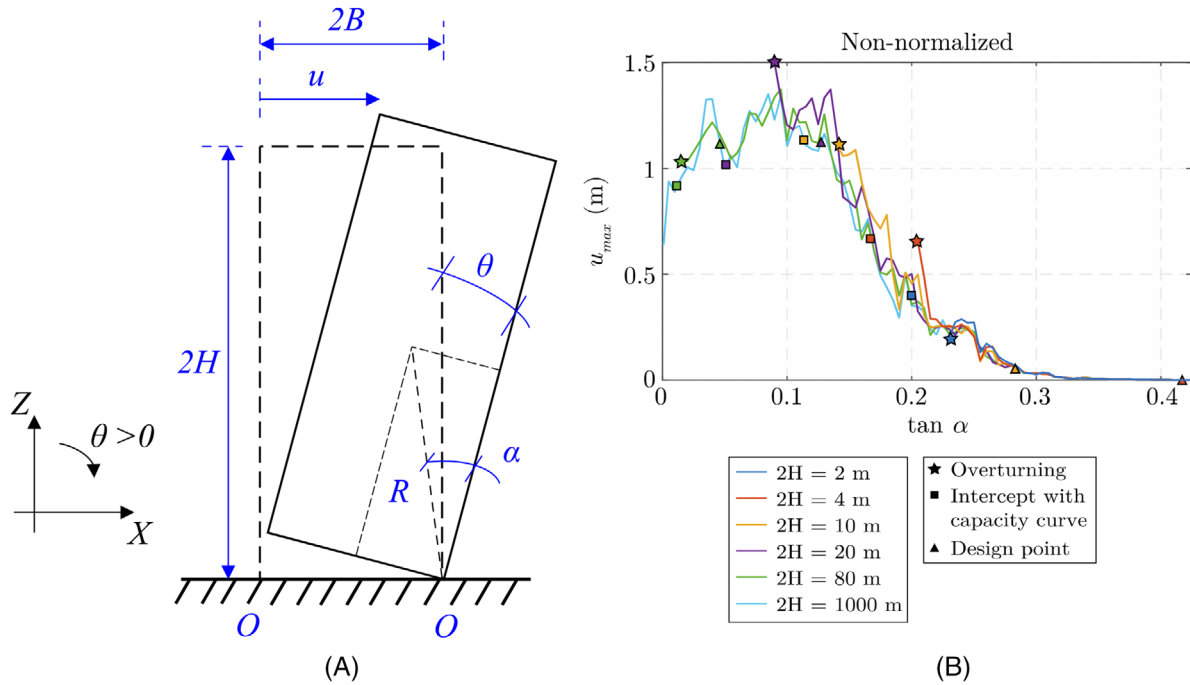


FIGURE 1 Displacement-based analysis of rocking blocks: (A) geometry of the rigid rocking block showing angle of rotation ( $\theta$ ) and horizontal displacement ( $u$ ) (B) median rocking displacement spectra median for different sizes for a set of near-field pulse-like records.<sup>65</sup>

$T$ , for several values of  $\zeta$ . This does not hold for the rocking oscillator, where the tilt angle response strongly depends on both parameters  $\alpha$  and  $R$ , hindering the creation of univariate spectra of maximum tilt angle response.

Reggiani Manzo and Vassiliou<sup>65,66</sup> suggested that using displacements instead of tilt angles can reduce the dimensionality of the rocking oscillator problem. The top displacement,  $u$ , of the rocking block can be obtained by a one-to-one mapping of rotation,  $\theta$ , (see Figure 1A):

$$u = 2R \sin(\pm\alpha) - 2R \sin(\pm\alpha - \theta) \quad (3)$$

They showed that a displacement-based description of the rocking problem uncovers that a large and a small rocking block of the same slenderness will have roughly the same top displacement, if they both are away from overturning. They named this conclusion “*equal displacement rule of rocking structures*.” Therefore, the maximum of the displacement time history of any block of slenderness  $\alpha$  can be approximated by calculating the response of an infinitely large (so that it does not overturn) block of slenderness  $\alpha$ . Such an approximation becomes more accurate when the comparison is performed in the statistical sense, that is, by comparing median responses to sets of ground motions, rather than responses to individual ground motions. Figure 1B is reproduced from<sup>65</sup> and it offers such rocking displacement spectra (i.e., the temporal maximum of the displacement as a function of the slenderness  $\alpha$  for different block sizes). The offered spectra concern the median response to a set of four near field pulse like ground motions.

Therefore, to study the effect of different correction schemes on rocking structures, one can study the response of infinitely large rocking blocks, so that the dimensionality of the problem is reduced by one. Then, displacement spectra for different correction methods can be compared. For numerical reasons, this paper will approximate the  $2H \rightarrow \infty$  case by blocks with height equal to  $2H = 2000$  m.

### 3 | SOURCES OF NOISE AND TYPICAL CORRECTION PROCEDURES

In 1932, the first accelerographs were developed in the US leading to the first strong motion accelerograms of the Long Beach (California) earthquake (March 1933).<sup>3</sup> Ever since, the number of installed accelerographs around the world has rapidly increased. Figure 2 shows the development of the number/percentage of digital and analog records based on the NGA West 2 database flatfile.<sup>67</sup> The figure shows that digital records were introduced in around 1980 and their share rapidly grew until around the year 2000 when 100% of the recordings became digital.

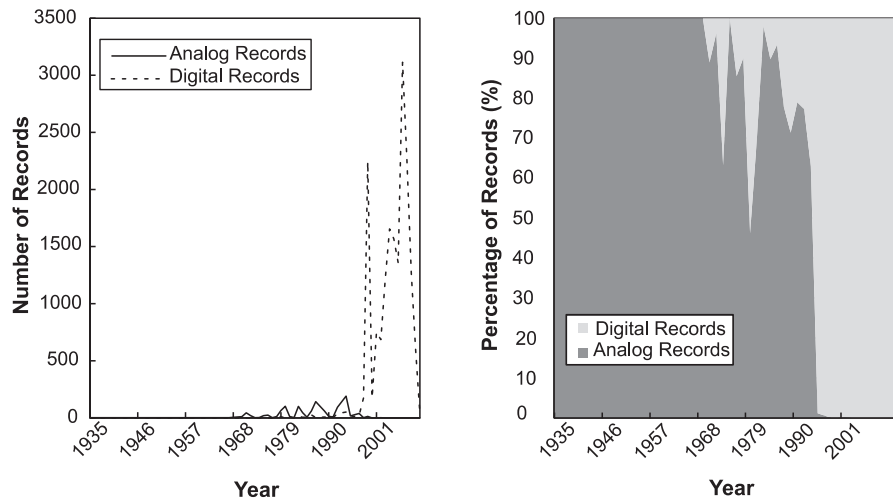


FIGURE 2 Development of the number/percentage of digital and analog records based on the NGA West 2 database flatfile.<sup>67</sup>

Analog devices record the ground acceleration against time on a film or paper. Disadvantages of such analog recording devices include the relatively low natural frequency (typically 25 Hz) that results in a relatively low upper bound of the frequencies they can measure with confidence, the need for digitization, and the use of an acceleration trigger. The need for an acceleration threshold for starting the record stems from limited recording medium and results in losing the first part of the motion where the motion intensity is below the threshold. On the other hand, digital recorders have generally higher natural frequency (50–100 Hz) and are able to record pre-event motion that may help in understanding of the nature of noise. They also omit the need for digitization, which is a significant source of noise in analog recorders. Nevertheless, digital recordings still contain distortions that require processing.<sup>3,4</sup> Boore and Bommer<sup>3</sup> claimed that, despite their disadvantages, analog records constitute and will continue to constitute an important part of ground motion databases until they become redundant by digital recordings. Acknowledging that, nearly half of the ground motions used in this study were from analog devices in order to compare with digital recordings.

The nature of noise and baseline tilts in analog recordings are very distinct from digital records.<sup>3</sup> As discussed earlier, the noise is easier to detect in displacement and velocity time series. To better explain the different nature of noise, Figure 3 depicts the unprocessed/unfiltered acceleration, velocity, and displacement traces, as well as the acceleration Fourier Amplitude Spectrum (FAS) for two stations from the 1994 Northridge, California earthquake. The two stations are Tarzana Cedar Hill Nursery A and Los Angeles (Temple & Hope) which were recorded on analog and digital instruments, respectively. Investigating the velocity traces in Figure 3, the velocity trace of the analog record (Figure 3A) starts at zero, then it peaks in the middle (at about 13 s) and then returns back to zero. In contrast, the velocity trace of the digital record (Figure 3B) appears to have a linearly increasing baseline offset that starts at roughly 10 seconds.

Noise can also result into unphysical Fourier Amplitude Spectra (FAS). Seismological theory dictates that at low frequencies, the FAS of acceleration should decay with decreasing frequency.<sup>3,68,69</sup> Figure 3 (right), shows that the analog record appears to start deviating from the required descending trend in the low frequency range at higher frequencies (around 1 Hz) than digital record (around 0.08 Hz).

These observations emphasize the higher difficulty of correcting analog records and the limited information that an engineer can acquire from them at long periods which is mostly important for long span bridges or isolated structures.

Based on the above, raw ground motions, extracted directly from digital sensors or digitized from analog records, typically include both low and high frequency noise. Processing of strong ground motions aim at creating zero final velocity and residual displacement that matches geodetic recordings. It typically starts with removing the mean value of the pre-event buffer (or the mean of the whole record in case pre-event data are not available, which is the case in analog ground motion records).<sup>1,70,71</sup> The next step is to apply a low and high pass Butterworth filters. As earthquake engineers are used to periods, not to frequencies, it needs to be clarified that this paper follows the typical terminology of signal processing, that is “low” and “high” refer to frequencies. Therefore, a high-pass filter (low-cut filter) removes the low frequency / long period noise.

Two types of filters are typically used: causal and acausal (zero-phase) filters. Causal filters result in shifted filtered ground motion signal in contrast to acausal filters. Acausal filters is the state of the art within ground motion processing

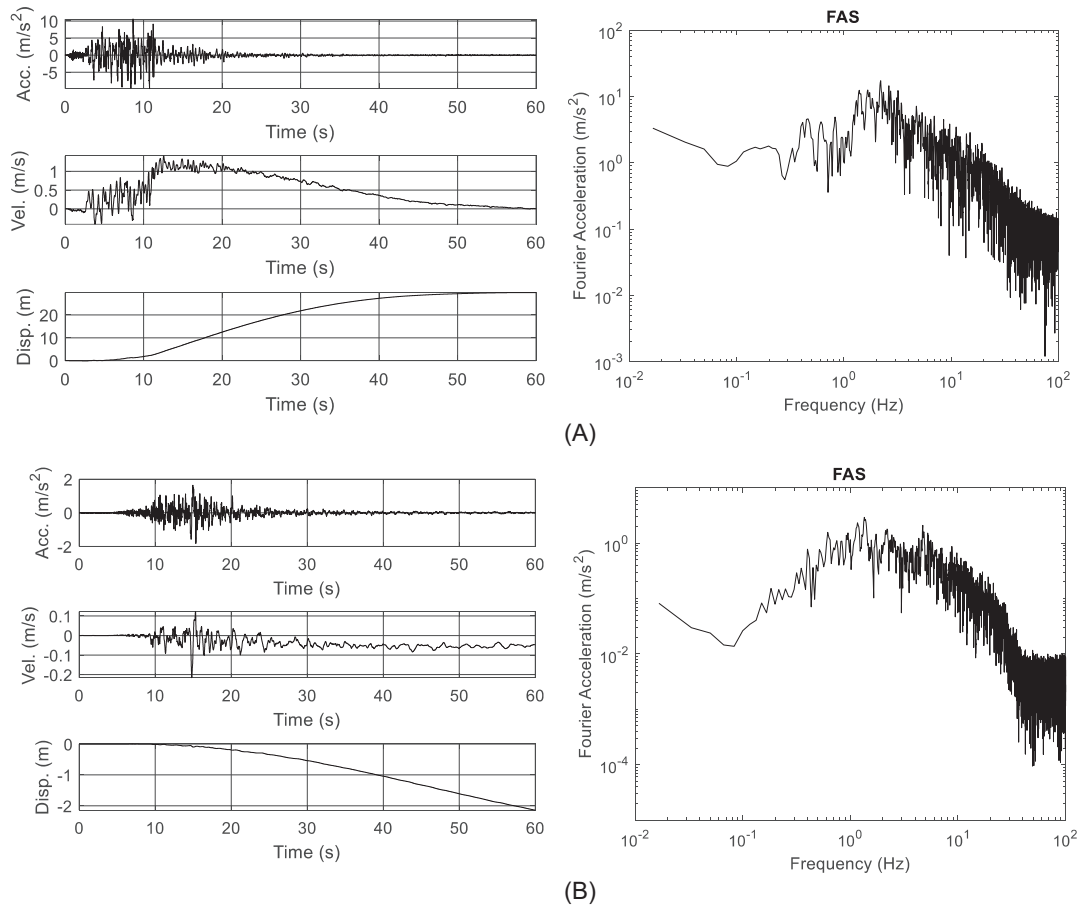


**FIGURE 3** Unprocessed/Unfiltered acceleration, velocity, and displacement traces and acceleration Fourier Amplitude Spectrum (FAS) for (A) analog record: 1994 Northridge EQ (station: Tarzana Cedar Hill Nursery A) (B) digital record: 1994 Northridge EQ (station: Los Angeles—Temple & Hope)

context. NGA West 1 project used causal filtered ground motions, while acausal filters were used in the updated version of the project, NGA West 2.<sup>72</sup> The choice of filter parameters (order and corner frequency) involves some degree of subjective judgement since the noise source is not well understood, especially the long period noise.<sup>3</sup> The decisions on filter parameters is based on iterations aiming at obtaining reasonable ground motion traces. Boore and Bommer<sup>3</sup> claimed that it is impossible to identify an optimal processing technique for an individual ground motion and that the uncertainty of the whole procedure should be appreciated by the end users of the processed record.

#### 4 | DESCRIPTION OF THE GROUND MOTION DATABASE

The goal of the selection of ground motion records, in this study, was to cover different variations of instrument noise (analog and digital) and ground motion types (i.e., pulse like or no-pulse like). In total, 34 ground motions were selected and split into two main groups; analog (16 ground motions) and digital records (18 ground motions). Each group is split into three sub-groups as in FEMA P695<sup>73</sup> (near field pulse-like, near field no pulse-like, and far-field).

A source-site distance (defined as the Joyner-Boore distance<sup>74</sup>) of 10 km was used to separate near-field and far-field records. Only strong motions (magnitude > 6.5) were considered. For each ground motion, the two horizontal components were treated as different records, resulting in 67 records in total (for one ground motion only one component was used). The vertical component of the ground motion was not used in this study, as it seems that it does not significantly influence the response of the rocking oscillator.<sup>75–80</sup> The ground motions were classified as pulse-like or no pulse-like based on the classification of PEER NGA West 2 database, if the ground motion is available there. Otherwise, the methodology and the code developed by Shahi and Baker<sup>81,82</sup> are used to classify the ground motion.

TABLE 1 Analog records

Event	M	Station	Database	$R_{jb}$ (km)	PGA (m/s <sup>2</sup> )	PGV (m/s)	PGD (m)	Pulse/No-Pulse
1971 San Fernando	6.61	Lake Hughes #12	CESMD <sup>b</sup>	13.99	3.734	0.406	0.162	No-pulse
1992 Landers	7.28	Desert Hot Springs—Fire Station	CESMD	21.78	1.740	0.205	0.090	No-pulse
1989 Loma Prieta	6.93	Santa Cruz—UCSC Lick Elect. Shop	CESMD	12.04	4.409	0.228	0.076	No-pulse
		Gilroy #6 - San Ysidro Microwave Site	CESMD	17.92	1.701	0.149	0.056	No-pulse
1971 San Fernando	6.61	Pacoima Dam (upper left abut)	CESMD	0.00	11.671	1.683	0.763	Pulse-like
1989 Loma Prieta	6.93	Saratoga—Aloha Ave [aband]	CESMD	7.58	5.115	0.448	0.306	Pulse-like
		Saratoga - 1-story Gymnasium	CESMD	8.48	3.254	0.624	0.372	Pulse-like
1994 Northridge	6.69	Sylmar; Jensen Filter Plant; Admin. Bldg	CESMD	0.00	6.222	1.917	1.592	Pulse-like
		Newhall—County Fire Sta.	CESMD	3.16	5.931	0.965	0.393	Pulse-like
		Sylmar—Pacoima Dam Downstream	CESMD	4.92	4.398	0.473	0.067	Pulse-like
1989 Loma Prieta	6.93	Corralitos—Eureka Canyon Road	CESMD	0.16	6.339	0.573	0.183	No-pulse
		Capitola—Fire Station	CESMD	8.65	4.882	0.372	0.122	No-pulse
1994 Northridge	6.69	Arleta—Nordhoff Ave Fire Sta [aband]	CESMD	3.30	3.401	0.404	0.165	No-pulse
		Canoga Park; Santa Susana, Ground Station (ETEC)	CESMD	1.69	3.326	0.334	0.206	No-pulse
		Tarzana—Cedar Hill Nursery A [rplcd]	CESMD	0.37	18.301	0.909	0.544	No-pulse
Elcentro <sup>a</sup> 1940	6.90	El Centro #9 (station code: 117)	CESMD	6.09	3.105	0.429	0.443	No-pulse

<sup>a</sup>Only one horizontal component was used.

<sup>b</sup>CESMD: Center for Engineering Strong Motion Data,<sup>83</sup> with stations that belong to different networks including coast and geodetic survey (C&GS), California Strong Motion Instrumentation Program (CSMIP), and United States National Strong-Motion Network (NSMP).

Tables 1 and 2 summarize the ground motion database for analog and digital records, respectively. The PGA, PGV, and PGD values in Tables 1 and 2 are calculated using the records corrected using acausal filtering (discussed later in the paper) with a high-pass filter corner frequency 0.1 Hz. These values are taken as the maximum of the temporal maximum of each of the two horizontal components of each record, that is,  $PGA = \max(PGA_x, PGA_y)$ .

## 5 | ADOPTED PROCESSING SCHEMES

The processing scheme comprised a baseline correction and an application of a causal or acausal filter. Figure 4 depicts the adopted processing schemes for acausal filtering. The scheme was based on the NGA West 2 processing methodology.<sup>2,72</sup> It starts by removing the pre-event buffer mean in the case of digital records (or the record mean in case of analog records). Then the start and the end of the signal are tapered using cosine tapers with a length equal to 1% of the trace length.<sup>84</sup> The next step is to apply zero pads at the end of the record so that the number of points in the time series is a power of two since the filtering is conducted in the frequency-domain using the Fast Fourier transform (FFT).<sup>85</sup> Thereafter, high pass and low pass acausal Butterworth filters are applied to the acceleration time series in the frequency domain. Then, the zero pads are removed and a sixth-order polynomial is fitted to the displacement trace (obtained by double integration of the acceleration trace) and the second derivative of the polynomial is subtracted from the acceleration time history. A similar procedure was used for the causal filtering scheme with a causal Butterworth filter (Figure 5). For causal filters, the tapering and zero padding steps are not included since they are only needed for the acausal filtering.<sup>2,86</sup>

Apart from the baseline correction and filtering, the time series for all ground motion records were checked for non-standard noise (e.g., unrealistic spikes) on a single record basis.

The MATLAB code used in this study was based on the codes of Akkar<sup>87</sup> and Abrahamson.<sup>2</sup>

The used corner periods of the high-pass filters were 10, 15, 20, 30, 40, and 60 s, with longer periods corresponding to more relaxed filtering and shorter periods corresponding to more intense filtering. The chosen high-pass corner periods range was based on<sup>71</sup> in which the effects of long-period processing on structural collapse predictions of steel moment frames was investigated. The low-pass filter (causal and acausal) corner frequency was chosen to be 25 Hz (i.e., corner period equal to 0.04 s) based on the studies by.<sup>88–90</sup>

TABLE 2 Digital records

Event	M	Station		$R_{jb}$ (km)	PGA (m/s <sup>2</sup> )	PGV (m/s)	PGD (m)	Pulse/No-Pulse
1989 Loma Prieta	6.93	San Jose—Santa Teresa Hills	CESMD <sup>a</sup>	14.18	2.789	0.254	0.117	No-pulse
2010 El Mayor-Cucapah	7.20	El Centro—Imperial & Ross	CESMD	19.39	3.730	0.445	0.314	No-pulse
		Calexico; Fire Station	CESMD	19.12	2.559	0.206	0.106	No-pulse
1994 Northridge	6.69	Los Angeles—Temple & Hope	CESMD	27.82	1.816	0.199	0.036	No-pulse
		Los Angeles—Pico & Sentous	CESMD	28.82	1.824	0.140	0.041	No-pulse
		Lake Hughes #12A [abandoned]	CESMD	20.77	2.535	0.119	0.061	No-pulse
2008 Wenchuan, China	7.90	Mianzuqingping	NSMONS <sup>b</sup>	0.00	7.127	0.905	0.565	Pulse-like
1999 Chi-Chi, Taiwan	7.62	TCU049	TSMIP <sup>c</sup>	3.76	2.658	0.625	0.348	Pulse-like
		TCU068	TSMIP	0.00	5.014	1.560	1.401	Pulse-like
		TCU102	TSMIP	1.49	2.909	0.829	0.728	Pulse-like
		TCU082	TSMIP	5.16	2.119	0.431	0.378	Pulse-like
		TCU065	TSMIP	0.57	7.750	1.158	0.710	Pulse-like
2016 Kaikoura	7.80	KEKS	GeoNet <sup>d</sup>	3.00	10.909	1.054	0.453	No-pulse
		WDFS	GeoNet	8.50	12.232	0.922	0.348	No-pulse
		WTMC	GeoNet	0.70	10.345	1.064	0.367	No-pulse
2015 Nepal	7.80	KATNP	CESMD	0.10	1.655	0.983	0.843	No-pulse
2016 Kumamoto	7.00	KMM004	K-NET, KiK-net, and JMA <sup>e</sup>	3.90	3.439	0.777	0.457	No-pulse
		KMMH16		0.50	11.574	1.343	0.455	No-pulse

<sup>a</sup>See footnote 1 for Table 1.

<sup>b</sup>NSMONS: National Strong-Motion Observation Network System of China.

<sup>c</sup>TSMIP: Taiwan Strong Motion Instrumentation Program.

<sup>d</sup>GeoNet: The New Zealand GeoNet project.

<sup>e</sup>K-NET, KiK-net: Japan network of strong-motion seismographs, JMA: Japan Meteorological Agency.

Figure 6 shows the filter frequency response function (magnitude and phase) for the adopted causal and acausal (zero phase) filters with eight poles for different cut-off periods. The figure depicts the difference in phase shifts between causal and acausal filters as discussed earlier. It is also worth mentioning that discussions about usable spectral periods (often expressed relative to the filter corner period, similar to the studies by<sup>68,91</sup> among others) are irrelevant to the rocking oscillator since its “period” is amplitude dependent and can take values from zero to infinity.<sup>5</sup>

As an example, Figure 7 shows the corrected time series for one of the 1989 Loma Prieta earthquake records (analog record at station: Capitola-Fire Station) using the correction algorithms adopted in this paper. The velocity and displacement traces indicate that the corner period of the filter influences the output signal more when causal filters are used. This is mainly due to phase shifts associated with causal filtering.

As a verification of the code developed for this paper, Figure 8 compares the same corrected ground motion (1989 Loma Prieta earthquake, Capitola station) to the corrected record acquired from the PEER NGA West 2 project.<sup>72</sup> Although the match is not perfect, the differences are small and the results satisfy the main goals of ground motion correction (reasonable velocity and displacement traces). It is worth mentioning that the PEER ground motion correction software is not publicly available and the processing is performed via an external contractor. Moreover, Boore et al.<sup>2</sup> did not have access to the correction software used by the contractor doing the ground motion processing for PEER and had to develop their own code. Notably, in this study, the Zero Order Corrected (ZOC) record refers to the record with mean removed (mean of the whole record or the pre-event portion as discussed earlier).

## 6 | ROCKING SPECTRA RESULTS

As discussed earlier, the rocking spectra presented in this study plot the maximum top displacement of a rigid block versus the tangent of the slenderness angle. Accordingly, the rocking spectrum is not to be confused with the linear elastic



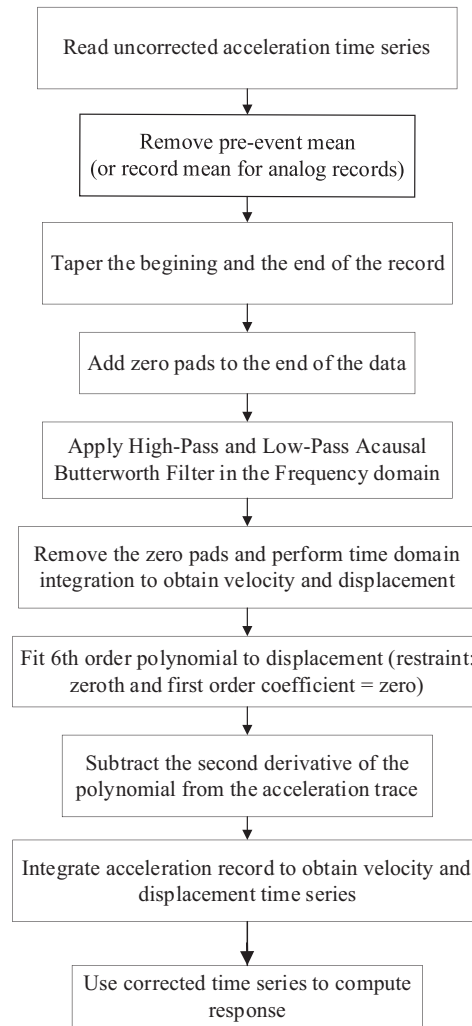


FIGURE 4 The adopted processing algorithm for acausal filtering based on the PEER NGA West 2 processing scheme.<sup>2,72</sup>

oscillator spectrum (elastic spectrum). The rocking spectrum is highly non-linear and is not correlated to the elastic spectrum.<sup>11</sup> For reasons that will be discussed later in this section, all ground motions were scaled to have a PGV of 50 cm/s. As the raw ground motion results in unrealistically high PGVs, the scaling factor for different corner periods and for the same component was kept constant and equal to the one needed to scale the record that was processed with the 10 s cut off period and an acausal filter to a PGV of 50 cm/s. As the number of analyses was high, the ETH Zurich scientific computing cluster (Euler) was used for performing the analysis.

Figure 9 shows some indicative rocking spectra for causal and acausal filtering. To develop Figure 9, the recordings at the following stations were used: Desert Hot Springs for Landers earthquake, Pacoima Dam for San Fernando earthquake, El Centro for El Mayor Cucapah earthquake, and WTMC for Kaikoura earthquake. One can observe that causal filtering resulted in higher variability than acausal filtering, an observation that agrees with previous studies for elastic systems.<sup>86</sup> In addition, in all cases in Figure 9, the variability of the spectrum due to the choice of different cut-off frequencies decreases with increasing tangent of the slenderness angle  $\alpha$ . There is a physical reason for this: As the slenderness angle decreases, the rocking block tilts to larger angles. Larger tilt angles lead to larger periods,<sup>5</sup> where the variability due to high-pass filtering typically is expected to increase, as in elastic systems.<sup>86,92</sup>

The discussion up till this point only focused on the spectra on a single ground motion basis. As rocking is a very sensitive problem, to all the parameters that define it, Yim et al.,<sup>93</sup> as early as 1980, have suggested that a sensitivity analysis of the rocking oscillator should be performed in a statistical sense, namely by comparing the statistics of the response to an ensemble of ground motions, rather than to individual excitations. Such a statistical approach is not only applied to rocking structures: Riddell and Newmark<sup>94</sup> produced inelastic spectra for yielding structures based on statistics on ensembles of

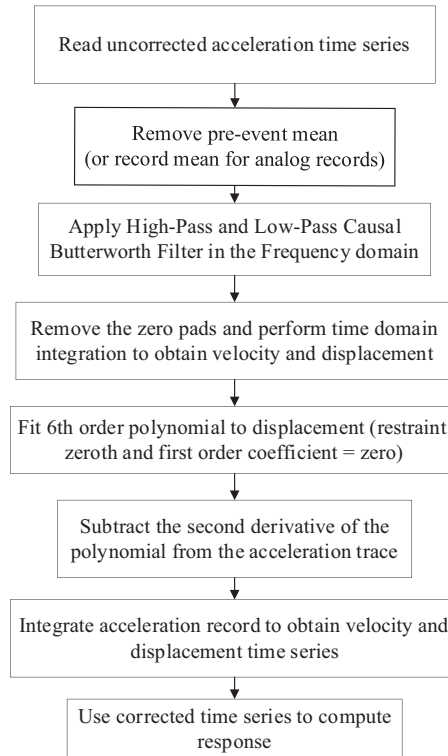


FIGURE 5 The adopted processing algorithm for causal filtering

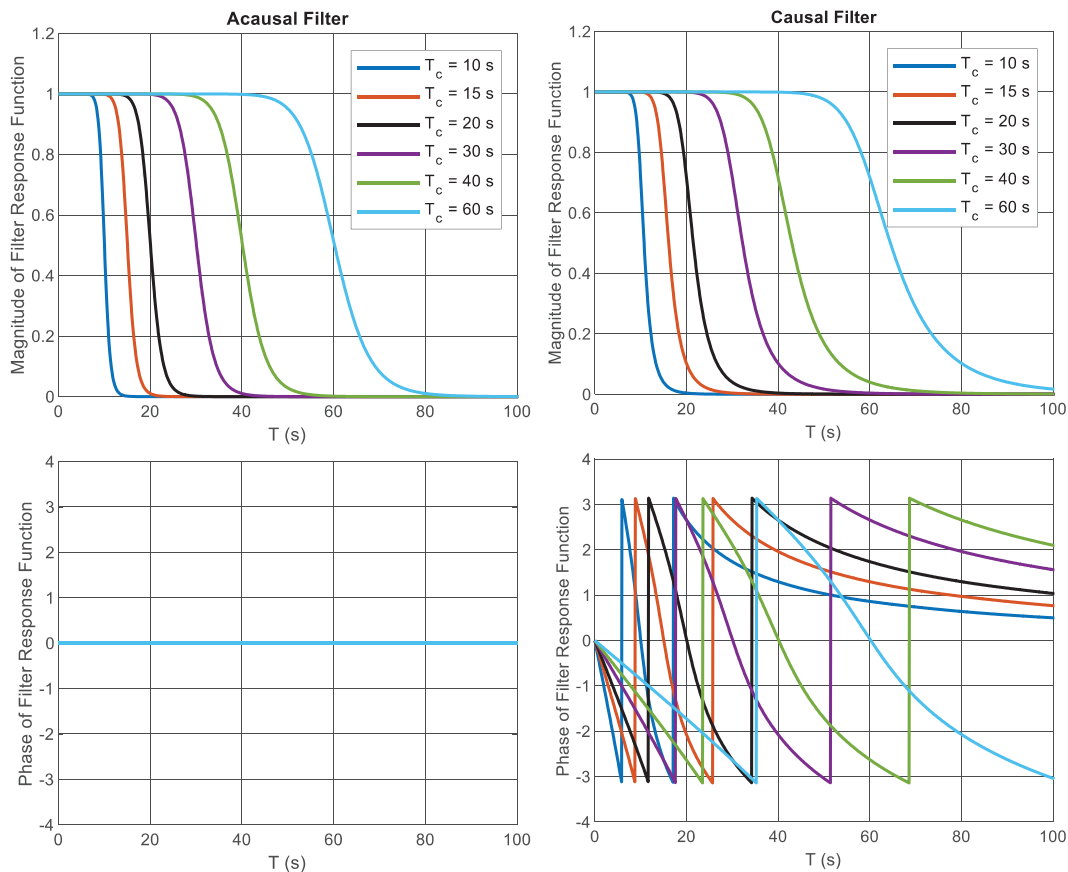
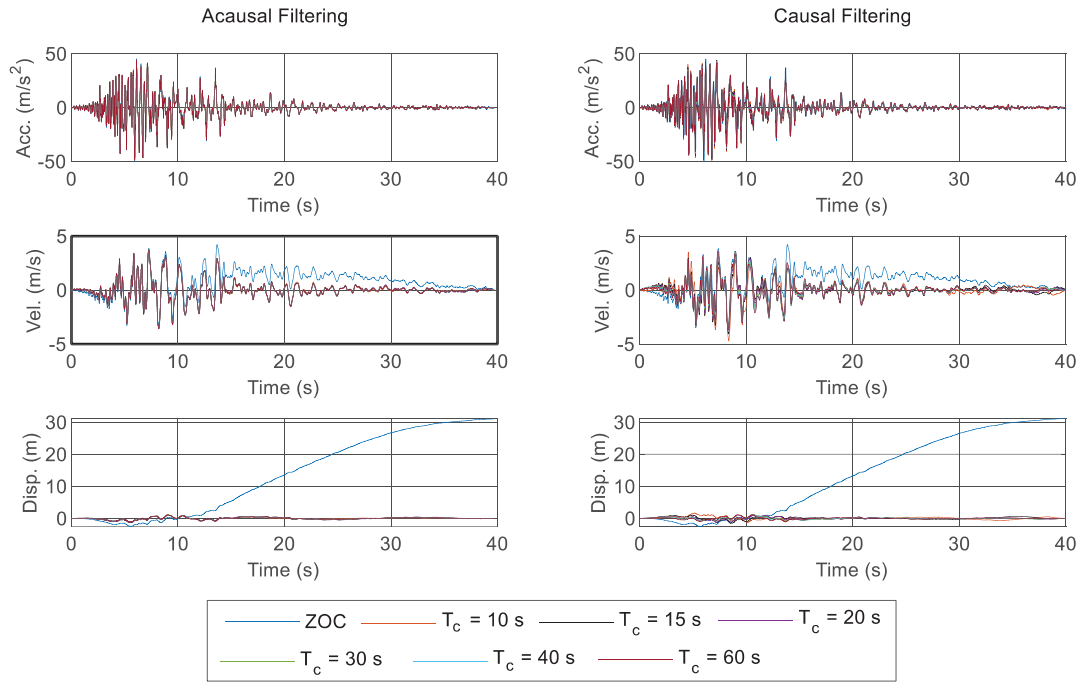
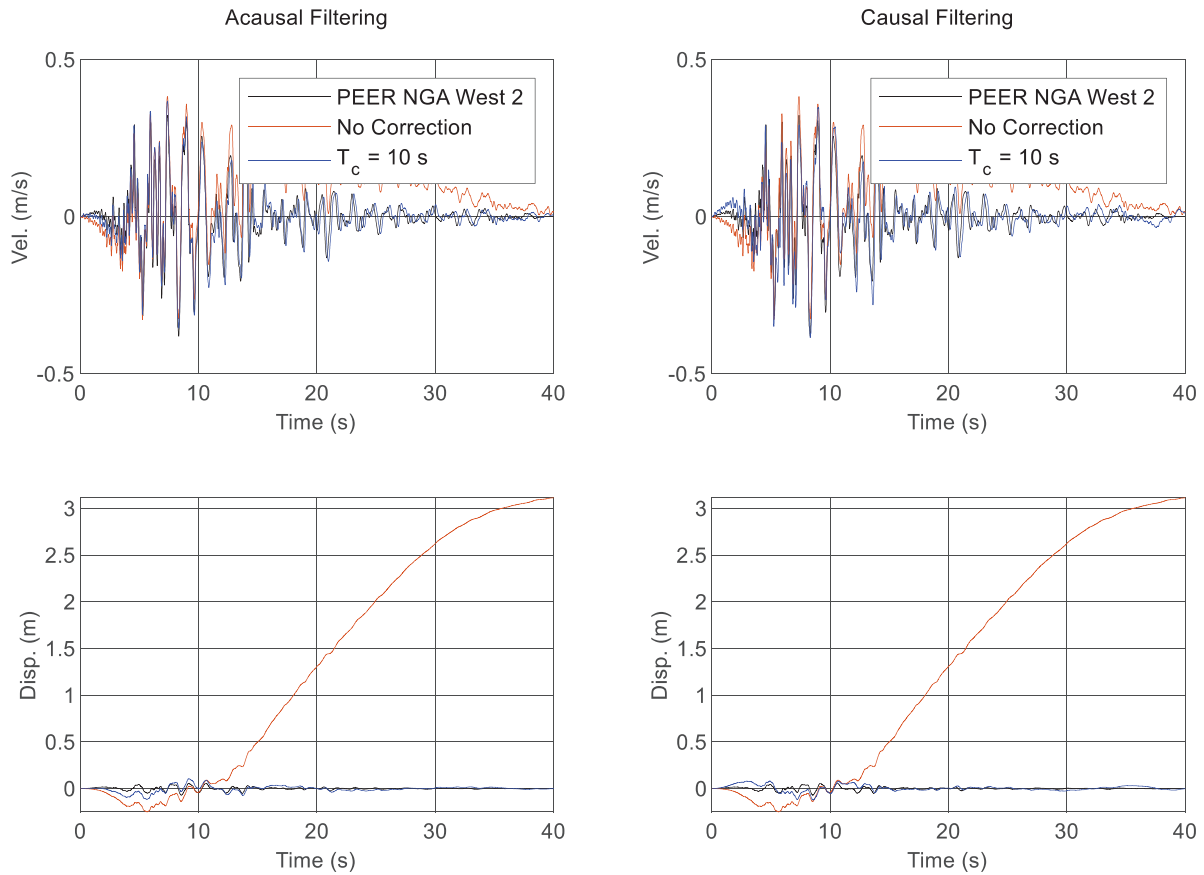


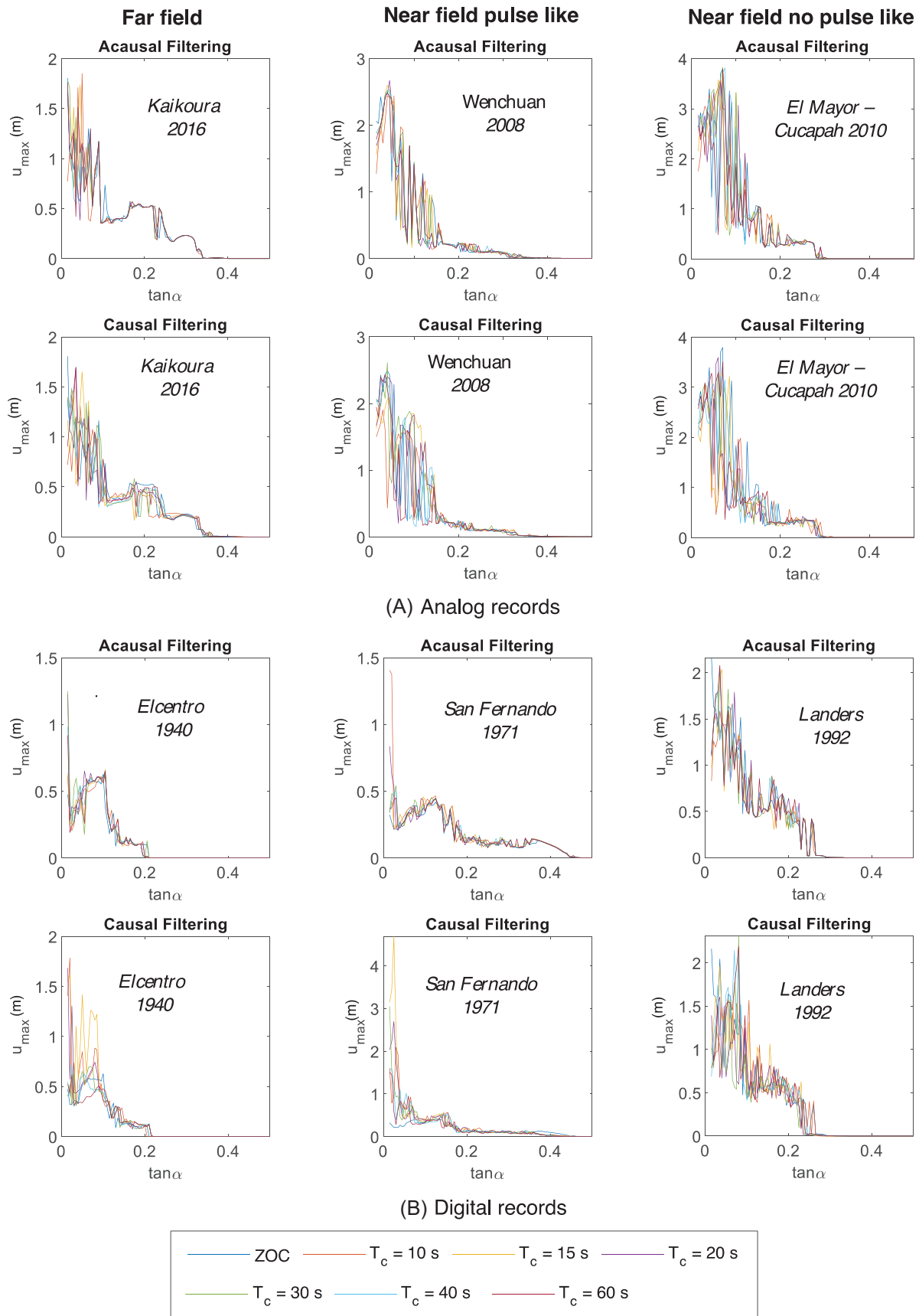
FIGURE 6 Filter response function (magnitude and phase in radian) of the adopted acausal (zero phase) and causal high-pass filters (number of poles = 8)



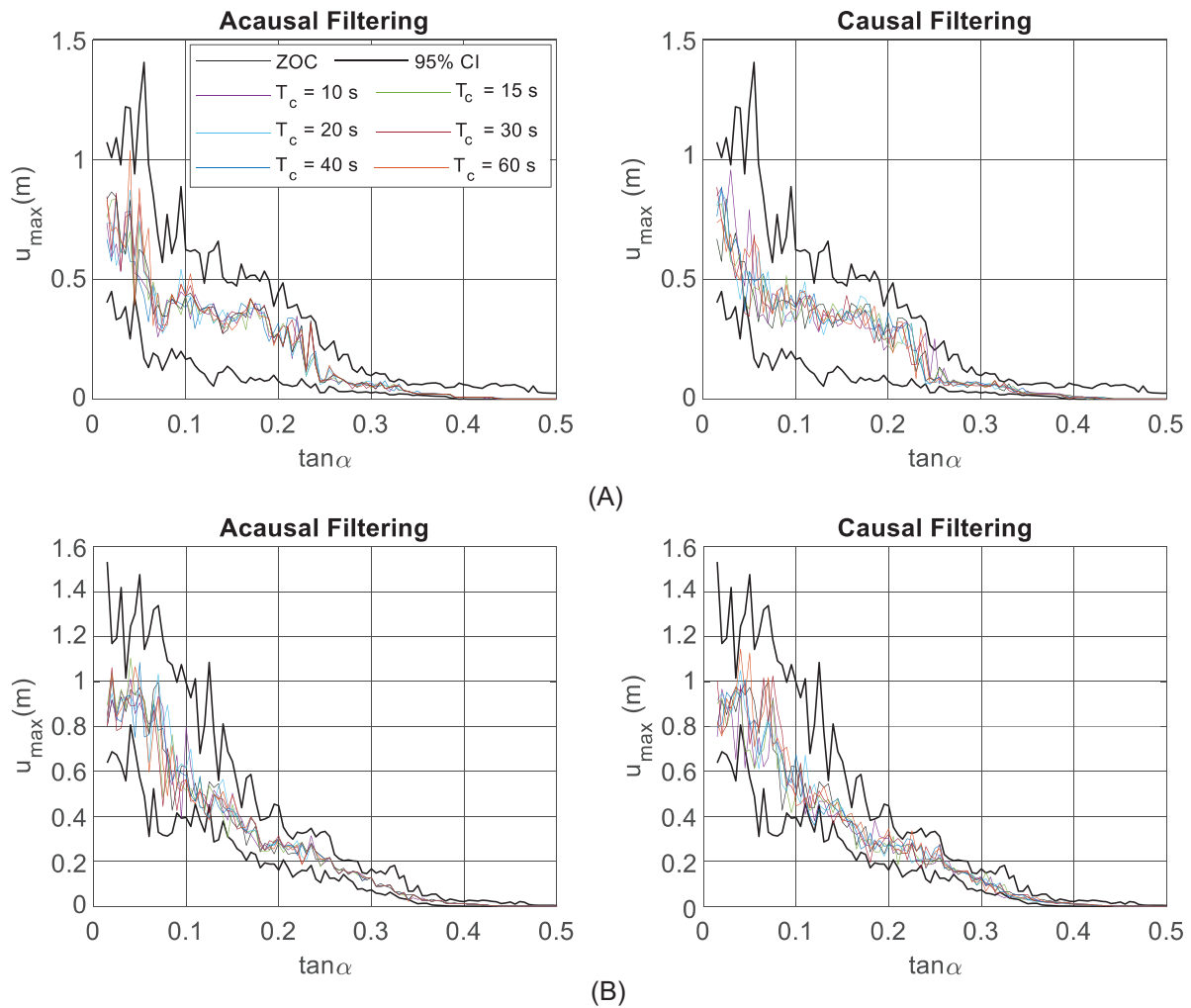
**FIGURE 7** Example of the corrected time series for one of the 1989 Loma Prieta earthquake records (analog record at station: Capitola—Fire Station)



**FIGURE 8** Comparison between the corrected ground motion using the adopted causal and acausal schemes with the corrected ground motion acquired from the PEER NGA West 2 database for the 1989 Loma Prieta earthquake (analog record at station: Capitola—Fire Station)



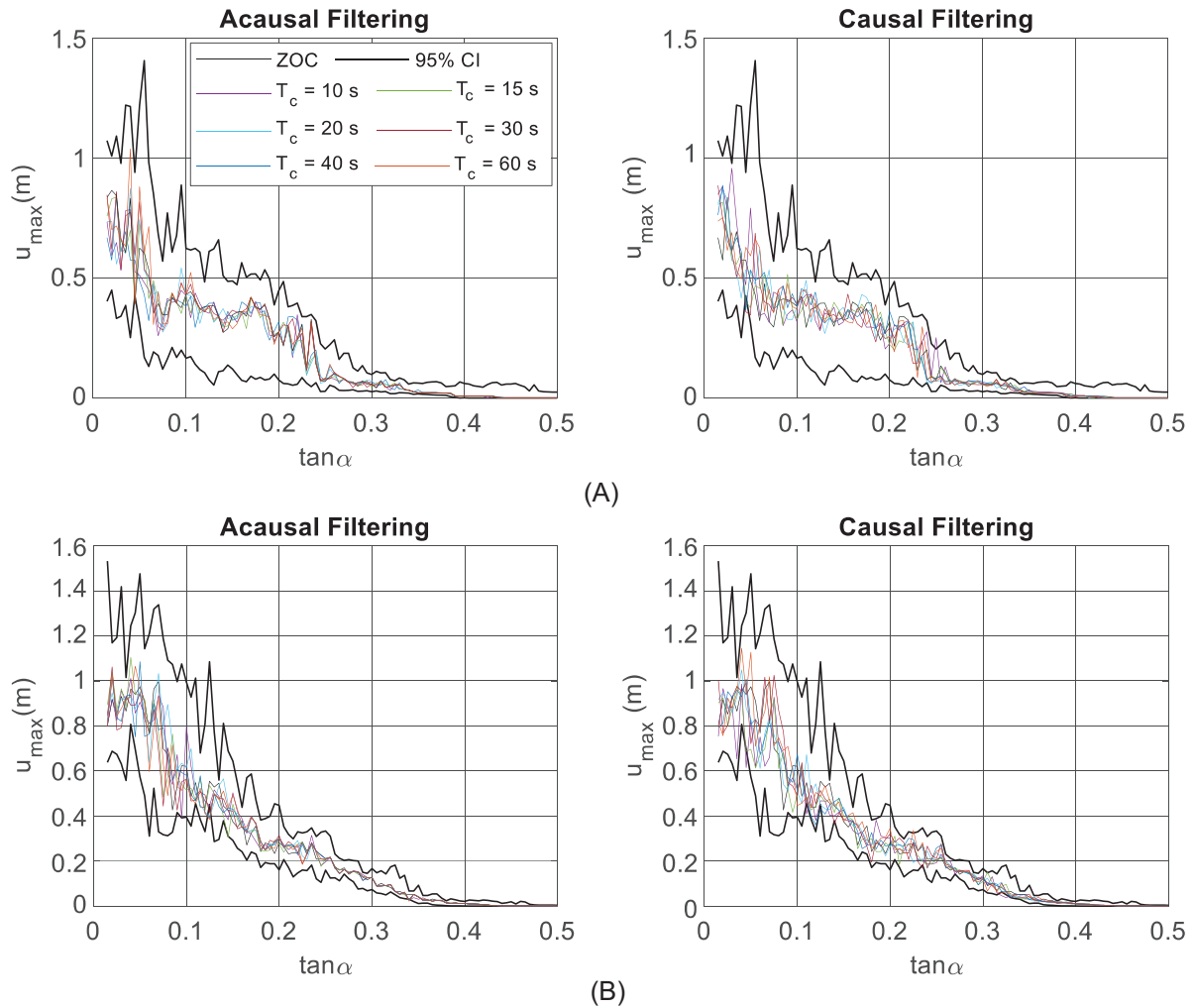
**FIGURE 9** Example rocking spectra for different categories of filtering schemes and ground motions for (A) Analog ground motion records (B) digital ground motion records (left: far field, middle: near field pulse like, right: near field no pulse-like)



**FIGURE 10** Median estimates of the rocking spectra for different correction schemes for the *far-field* record set (A) analog record set and (B) digital record set (the confidence interval is derived for the ZOC spectrum)

excitations. In fact, this approach is consistent with the fundamental seismic design problem, which involves computing the response to a set of ground motions, rather than to an individual one.<sup>95-103</sup>

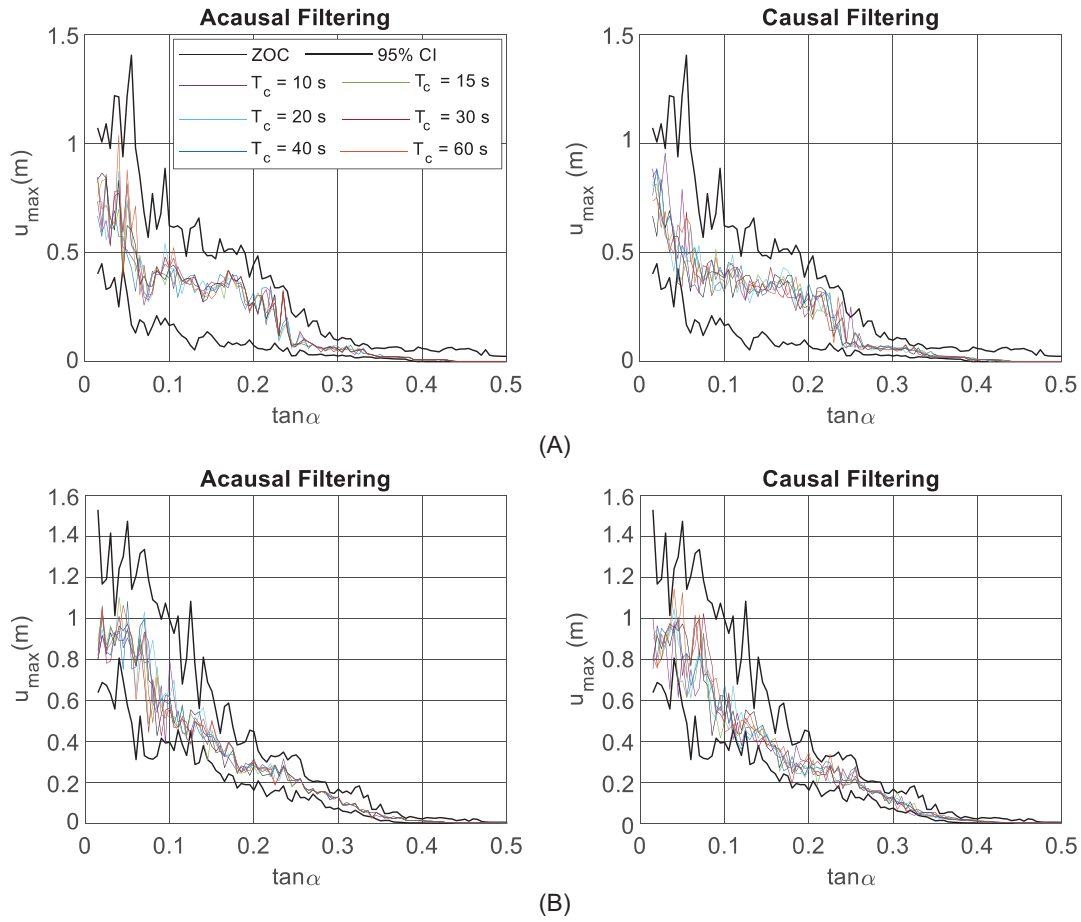
For an ensemble of ground motions to be useful, in this paper all ground motions were scaled to the same PGV. PGV was used as an intensity measure, as it performs better than PGA or PGD for rocking structures.<sup>104-111</sup> Figures 10, 11, and 12 show the median rocking spectra for the *far-field*, *near-field* pulse-like, and *near-field* no pulse-like record bins, derived for different processing schemes. As stated earlier, all the rocking spectra in this paper are derived for size ( $2H$ ) of 2000 m, which represent the case when  $2H \rightarrow \infty$  that is being studied for mathematical completeness. Then, these rocking spectra could be used to determine the response of rocking blocks of finite size, as shown in.<sup>65</sup> Moreover, Figures 10, 11, and 12 show the 95% confidence interval of the median (over the ground motions of each set) response for the zero-order corrected case (ZOC), that is, of the case where only the mean of the record was removed. The 95% confidence interval (CI) was constructed using the bootstrap method<sup>112</sup> by taking 1000 response samples for each value of  $\tan \alpha$ . Taking 10,000 response samples did not seem to change the CIs. Bootstrapping is a resampling with replacement method that can be used to estimate population statistics such as mean, standard deviation, and confidence intervals. This method is performed by selecting a sample having a number of datapoints (displacement responses, in this paper) equal to the original number of datapoints (some datapoints might be repeated, some will not exist in the new sample). This procedure is repeated  $n$  times (1000, in this paper) and the statistics of these  $n$  times represent the statistics of population of the quantity under investigation<sup>112</sup>.



**FIGURE 11** Median estimates of the rocking spectra for different correction schemes for the *near-field pulse-like* record set (A) analog record set and (B) digital record set (the confidence interval is derived for the ZOC spectrum)

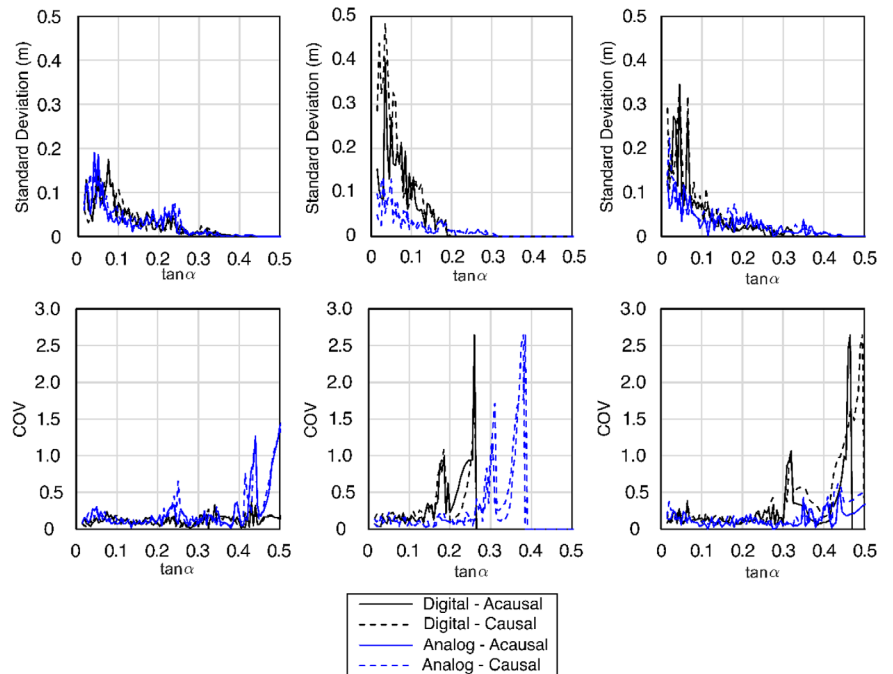
Based on the median rocking spectra (Figures 10–12), one can observe that for larger  $\tan\alpha$  (resulting into smaller displacements) the rocking spectra only loosely depend on the processing scheme, as it can also be observed on an individual motion base (Figure 9). For smaller  $\tan\alpha$ , there seems to be some non-negligible influence of the response on the processing scheme, but in most cases, the curves for the different processing schemes fall within the 95% confidence interval of the rocking spectrum of the zero-order corrected (ZOC) case, indicating that the motion-to-motion variability is larger than the variability caused by the different correction schemes. Moreover, there is no trend of the response with respect to increasing or decreasing corner period or with respect to causal or acausal filtering. Therefore, even if the different processing schemes do influence the rocking response, the bias of this influence seems negligible—at least for the parameter values examined. The above conclusion seems to be independent of whether the ground motion is pulse like or no pulse like and of the fault distance. It also holds for both analog and digital records.

Figure 13 shows the standard deviation and the coefficient of variation (COV, calculated as the standard deviation divided by the mean value) of the median estimates of the rocking spectra (Figures 10–12) for the cases presented in this study. The standard deviation values decrease for all the cases with increasing  $\tan\alpha$ , confirming that the variability decreases with  $\tan\alpha$ . For higher tangent of the slenderness angle, the COV reaches large values (on the order of 250%), but this only because in this region the mean tends to zero. Notably, for all the cases, the COV for the lower values of the tangent of the slenderness angle had almost a constant value of less than 0.2 on average.



**FIGURE 12** Median estimates of the rocking spectra for different correction schemes for the *near-field no pulse-like* record set (A) analog record set and (B) digital record set (the confidence interval is derived for the ZOC spectrum)

**FIGURE 13** Variability (standard deviation and coefficient of variation) of the median estimates of the rocking spectra for different processing schemes derived for the studies sets of ground motions (*left: far field, middle: near field pulse like, right: near field no pulse-like*)



## 7 | CONCLUSION

This study investigated the effect of ground motion processing (“correction”) on the response rocking structures. Different kinds of ground motions and variations of processing schemes were used to explore the effect on the rocking displacement spectra for planar rocking blocks. On a single ground motion basis, it can be concluded that:

- (i) Causal filtering results in higher variability than acausal filtering; agreeing with previous studies on the elastic oscillator.
- (ii) The variability of the spectrum due to the choice of different cut-off frequencies decreases with increasing tangent of the slenderness angle.

However, the seismic design problem does not involve the response to an individual ground motion but the statistics of the responses to a set of ground motions that characterize the seismic hazard. Therefore, this paper has argued that the influence of processing schemes should be evaluated statistically, essentially by evaluating whether they induce bias in the spectra. This work followed such an approach and showed that the median rocking displacement spectra to sets of ground motions are not significantly sensitive to the ground motion processing scheme. In most cases, the curves for the different processing schemes fall within the 95% confidence interval of the rocking spectrum of the zero-order corrected (ZOC) case. Therefore, the motion-to-motion variability was more important than the processing scheme. This conclusion holds for filter cut off periods larger than or equal to 10 seconds and applies to both analog and digital records, both causal and acausal filters, and to all near field pulse like, near field no pulse like, and far field records.

## ACKNOWLEDGMENTS

This work was supported by the ETH Zurich under grant ETH-11 21-1.

## DATA AVAILABILITY STATEMENT

The data that support the findings of this study are available from the corresponding author upon reasonable request.

## ORCID

Medhat Elmorsy  <https://orcid.org/0000-0002-2076-904X>

Michalis F. Vassiliou  <https://orcid.org/0000-0002-4590-2126>

## REFERENCES

1. Akkar S, Boore DM. On baseline corrections and uncertainty in response spectra for baseline variations commonly encountered in digital accelerograph records. *Bull Seismol Soc Am.* 2009;99(3):1671-1690.
2. Boore DM, Azari Sisi A, Akkar S. Using pad-stripped acausally filtered strong-motion data. *Bull Seismol Soc Am.* 2012;102(2):751-760.
3. Boore DM, Bommer JJ. Processing of strong-motion accelerograms: needs, options and consequences. *Soil Dyn Earthquake Eng.* 2005;25(2):93-115.
4. Boore DM, Stephens CD, Joyner WB. Comments on baseline correction of digital strong-motion data: examples from the 1999 Hector Mine, California, earthquake. *Bull Seismol Soc Am.* 2002;92(4):1543-1560.
5. Housner GW. The behavior of inverted pendulum structures during earthquakes. *Bull Seismol Soc Am.* 1963;53(2):403-417.
6. Chopra AK, Yim SC-S. Simplified earthquake analysis of structures with foundation uplift. *J Struct Eng.* 1985;111(4):906-930.
7. Psycharis IN. Effect of base uplift on dynamic response of SDOF structures. *J Struct Eng.* 1991;117(3):733-754.
8. Oliveto G, Calio I, Greco A. Large displacement behaviour of a structural model with foundation uplift under impulsive and earthquake excitations. *Earthq Eng Struct Dyn.* 2003;32(3):369-393.
9. Ma QTM. The mechanics of rocking structures subjected to ground motion. 2010, *ResearchSpace@ Auckland.*
10. Acikgoz S, DeJong MJ. The interaction of elasticity and rocking in flexible structures allowed to uplift. *Earthq Eng Struct Dyn.* 2012;41(15):2177-2194.
11. Makris N, Konstantinidis D. The rocking spectrum and the limitations of practical design methodologies. *Earthq Eng Struct Dyn.* 2003;32(2):265-289.
12. Stefanou I, Psycharis I, Georgopoulos I-O. Dynamic response of reinforced masonry columns in classical monuments. *Constr Build Material.* 2011;25(12):4325-4337.
13. DeJong MJ. Seismic response of stone masonry spires: analytical modeling. *Eng Struct.* 2012;40:556-565.
14. Tondelli M, Beyer K, DeJong M. Influence of boundary conditions on the out-of-plane response of brick masonry walls in buildings with RC slabs. *Earthq Eng Struct Dyn.* 2016;45(8):1337-1356.



15. Casapulla C, Giresini L, Lourenço PB. Rocking and kinematic approaches for rigid block analysis of masonry walls: state of the art and recent developments. *Buildings*. 2017;7(3):69.
16. Kalliontzis D, Schultz AE. Characterizing the in-plane rocking response of masonry walls with unbonded posttensioning. *J Struct Eng*. 2017;143(9):04017110.
17. Mehrotra A, DeJong MJ. The influence of interface geometry, stiffness, and crushing on the dynamic response of masonry collapse mechanisms. *Earthq Eng Struct Dyn*. 2018;47(13):2661-2681.
18. Prajapati S, Destro Bisol G, AlShawa O, Sorrentino L. Non-linear dynamic model of a two-bodies vertical spanning wall elastically restrained at the top. *Earthq Eng Struct Dyn*. 2022;51(11):2627-2647.
19. Vlachakis G, Giouvanidis AI, Mehrotra A, Lourenço PB. Numerical block-based simulation of rocking structures using a novel universal viscous damping model. *J Eng Mech*. 2021;147(11):04021089.
20. Kallioras S, Graziotti F, Penna A, Magenes G. Effects of vertical ground motions on the dynamic response of URM structures: comparative shake-table tests. *Earthq Eng Struct Dyn*. 2022;51(2):347-368.
21. Malomo D, DeJong MJ. A Macro-Distinct Element Model (M-DEM) for out-of-plane analysis of unreinforced masonry structures. *Eng Struct*. 2021;244:112754.
22. Konstantinidis D, Makris N. Experimental and analytical studies on the response of 1/4-scale models of freestanding laboratory equipment subjected to strong earthquake shaking. *Bull Earthquake Eng*. 2010;8(6):1457-1477.
23. Di Egidio A, Alaggio R, Contentob A, Tursinic M, Loggiac ED. Experimental characterization of the overturning of three-dimensional square based rigid block. *Internat J Non-Linear Mech*. 2015;69:137-145.
24. Wittich CE, Hutchinson TC. Shake table tests of stiff, unattached, asymmetric structures. *Earthq Eng Struct Dyn*. 2015;44(14):2425-2443.
25. Dar A, Konstantinidis D, El-Dakhkhni WW. Evaluation of ASCE 43-05 seismic design criteria for rocking objects in nuclear facilities. *J Struct Eng*. 2016;142(11):04016110.
26. Sextos AG, Manolis GD, Ioannidis N, Athanasiou A. Seismically induced uplift effects on nuclear power plants. Part 2: demand on internal equipment. *Nuclear Eng and Design*. 2017;318:288-296.
27. Dar A, Konstantinidis D, El-Dakhkhni W. Seismic response of rocking frames with top support eccentricity. *Earthq Eng Struct Dyn*. 2018;47(12):2496-2518.
28. Voyagaki E, Kloukinas P, Dietz M, et al. Earthquake response of a multiblock nuclear reactor graphite core: experimental model vs simulations. *Earthq Eng Struct Dyn*. 2018;47(13):2601-2626.
29. Di Sarno L, Magliulo G, D'Angela D, Cosenza E. Experimental assessment of the seismic performance of hospital cabinets using shake table testing. *Earthq Eng Struct Dyn*. 2019;48(1):103-123.
30. Liu P, Xue W, Pang H, Zhang YM, Chen HT, Yang WG. Seismic overturning fragility analysis for freestanding building contents subjected to horizontal bidirectional floor motions. *Soil Dyn Earthquake Eng*. 2022;161:107414.
31. Bao Y, Xu Y, Wu B. Modeling and validation of three-dimensional sliding-rocking rigid block subjected to earthquake excitation. *Earthq Eng Struct Dyn*. 2022;51(12):2858-2879.
32. Lu Y, Xiong F, Ran MM, Ge Q, Wang J. Seismic pounding damage to adjacent reinforced concrete frame-shear wall buildings and freestanding contents. *Earthq Eng Struct Dyn*. 2022;51(6):1436-1456.
33. Di Egidio A, Olivieri C, Contento A, Pagliaro S. Improving the dynamic and seismic behaviour of rigid block-like elements through active mass dampers. *Eng Struct*. 2023;275:115312.
34. Mouzakis HP, Psycharis IN, Papastamatiou DY, Carydis PG, Papantonopoulos C, Zambas C. Experimental investigation of the earthquake response of a model of a marble classical column. *Earthq Eng Struct Dyn*. 2002;31(9):1681-1698.
35. Papantonopoulos C, Psycharis IN, Papastamatiou DY, Lemos JV, Mouzakis HP. Numerical prediction of the earthquake response of classical columns using the distinct element method. *Earthq Eng Struct Dyn*. 2002;31(9):1699-1717.
36. Papaloizou L, Komodromos P. Planar investigation of the seismic response of ancient columns and colonnades with epistyles using a custom-made software. *Soil Dyn Earthquake Eng*. 2009;29(11-12):1437-1454.
37. Vassiliou MF, Makris N. Analysis of the rocking response of rigid blocks standing free on a seismically isolated base. *Earthq Eng Struct Dyn*. 2012;41(2):177-196.
38. Nikolić Ž, Krstevska L, Marović P, Smoljanović H. Experimental investigation of seismic behaviour of the ancient Protiron monument model. *Earthq Eng Struct Dyn*. 2019;48(6):573-593.
39. Makris N, Vassiliou MF. Planar rocking response and stability analysis of an array of free-standing columns capped with a freely supported rigid beam. *Earthquake Engng Struct Dyn*. 2013;42:431-449.
40. Makris N, Vassiliou MF. Are some top-heavy structures more stable? *J Struct Eng*. 2014;140(5):06014001.
41. Dimitrakopoulos EG, Giouvanidis AI. Seismic response analysis of the planar rocking frame. *J Eng Mech*. 2015;141(7):04015003.
42. Makris N, Vassiliou MF. Dynamics of the rocking frame with vertical restrainers. *J Struct Eng*. 2015;141(10):04014245.
43. Vassiliou MF, Makris N. Dynamics of the vertically restrained rocking column. *J Eng Mech*. 2015;141(12):04015049.
44. Agalianos A, Psychari A, Vassiliou MF, Stojadinovic B, Anastasopoulos I. Comparative assessment of two rocking isolation techniques for a motorway overpass bridge. *Front Built Environ*. 2017;3:47.
45. Giouvanidis AI, Dimitrakopoulos EG. Seismic performance of rocking frames with flag-shaped hysteretic behavior. *J Eng Mech*. 2017;143(5):04017008.
46. Vassiliou MF, Mackie KR, Stojadinović B. A finite element model for seismic response analysis of deformable rocking frames. *Earthquake Eng Struct Dyn*. 2017;46(3):447-466.

47. Vassiliou MF, Burger S, Egger M, Bachmann JA, Broccardo M, Stojadinovic B. The three-dimensional behavior of inverted pendulum cylindrical structures during earthquakes. *Earthq Eng Struct Dyn*. 2017;46(14):2261-2280.
48. Reyes SI, Almazán JL. A novel device for a vertical rocking isolation system with uplift allowed for industrial equipment and structures. *Eng Struct*. 2020;214:110595.
49. Vassiliou MF. Seismic response of a wobbling 3D frame. *Earthq Eng Struct Dyn*. 2018;47(5):1212-1228.
50. Du XL, Zhou YL, Han Q, Jia ZL. Shaking table tests of a single-span free-standing rocking bridge for seismic resilience and isolation. *Adv Struct Eng*. 2019;22(15):3222-3233.
51. Makris N, Aghagholizadeh M. Effect of supplemental hysteretic and viscous damping on rocking response of free-standing columns. *J Eng Mech*. 2019;145(5):04019028.
52. Thiers-Moggia R, Málaga-Chuquitaype C. Seismic protection of rocking structures with inerters. *Earthquake Engng Struct Dyn*. 2019;48(5):528-547.
53. Xie Y, Zhang J, DesRoches R, Padgett JE. Seismic fragilities of single-column highway bridges with rocking column-footing. *Earthq Eng Struct Dyn*. 2019;48(7):843-864.
54. Zhang J, Xie Y, Wu G. Seismic responses of bridges with rocking column-foundation: a dimensionless regression analysis. *Earthq Eng Struct Dyn*. 2019;48(1):152-170.
55. Giouvanidis AI, Dong Y. Seismic loss and resilience assessment of single-column rocking bridges. *Bull Earthq Eng*. 2020;18:4481-4513.
56. Sieber M, Klar S, Vassiliou MF, Anastasopoulos I. Robustness of simplified analysis methods for rocking structures on compliant soil. *Earthq Eng Struct Dyn*. 2020;49(14):1388-1405.
57. Thiers-Moggia R, Málaga-Chuquitaype C. Seismic control of flexible rocking structures using inerters. *Earthquake Engng Struct Dyn*. 2020;49(14):1519-1538.
58. Thomaidis IM, Kappos AJ, Camara A. Dynamics and seismic performance of rocking bridges accounting for the abutment-backfill contribution. *Earthq Eng Struct Dyn*. 2020;49(12):1161-1179.
59. Reggiani Manzo N, Vassiliou MF. Cyclic tests of a precast restrained rocking system for sustainable and resilient seismic design of bridges. *Eng Struct*. 2020;252:113620.
60. Thomaidis I, Camara Casado A, Kappos A. Dynamics and seismic performance of asymmetric rocking bridges. *J Eng Mech*. 2021;178(3):04022003.
61. Lu Y, Xiong F, Zhong J. Uniaxial hysteretic spring models for static and dynamic analyses of self-centering rocking shallow foundations. *Eng Struct*. 2022;272:114995.
62. Lin CP. *Base-Modified Post-Tensioned Rocking Walls for Tailored Seismic Response and Damage Reduction (Doctoral dissertation)*. University of Washington; 2022.
63. Zhang Y, Thiers-Moggia R, Málaga-Chuquitaype C. Impact and clutch nonlinearities in the seismic response of inerto-rocking systems. *Bull Earthquake Eng: SI: Advances on Inerter-based Seismic Protection of Structures*. 2022:1-33.
64. Reyes SI, Almazán JL, Vassiliou MF, Tapia NF, Colombo JI, de la Llera JC. Full-scale shaking table test and numerical modeling of a 3000-liter legged storage tank isolated with a vertical rocking isolation system. *Earthq Eng Struct Dyn*. 2022;51(6):1563-1585.
65. Reggiani Manzo N, Vassiliou MF. Displacement-based analysis and design of rocking structures. *Earthq Eng Struct Dyn*. 2019;48(14):1613-1629.
66. Reggiani Manzo N, Vassiliou MF. Simplified analysis of bilinear elastic systems exhibiting negative stiffness behavior. *Earthq Eng Struct Dyn*. 2021;50(2):580-600.
67. PEER. *PEER NGA West 2 Database Flatfile*, Pacific Earthquake Engineering Center (PEER).
68. Atkinson GM, Silva W. Stochastic modeling of California ground motions. *Bull Seismol Soc Am*. 2000;90(2):255-274.
69. Atkinson GM, Boore DM. Ground-motion relations for eastern North America. *Bull Seismol Soc Am*. 1995;85(1):17-30.
70. Lin Y, Zong Z, Tian S, Lin J. A new baseline correction method for near-fault strong-motion records based on the target final displacement. *Soil Dyn Earthquake Eng*. 2018;114:27-37.
71. Buyco K, Roh B, Heaton TH. Effects of long-period processing on structural collapse predictions. *Earthquake Spectra*. 2021;37(1):204-234.
72. Ancheta TD, Darragh RB, Stewart JP, et al. *PEER NGA-West2 Database*. Pacific Earthquake Engineering Research Center, University of California; 2013:134.
73. FEMA P695. *Quantification of Building Seismic Performance Factors*. Rep. FEMA P695, Federal Emergency Management Agency; 2009.
74. Abrahamson NA, Shedlock KM. Overview. *Seismol Res Lett*. 1997;68(1):9-23.
75. Ishiyama Y. Motions of rigid bodies and criteria for overturning by earthquake excitations. *Earthq Eng Struct Dyn*. 1982;10(5):635-650.
76. Shi B, Anoooshehpour A, Zeng Y, Brune JN. Rocking and overturning of precariously balanced rocks by earthquakes. *Bull Seismol Soc Am*. 1996;86(5):1364-1371.
77. Makris N, Zhang J. *Rocking Response and Overturning of Anchored Equipment Under Seismic Excitation [rep. no. PEER 1999-06]*. Pacific Earthquake Engineering Research Center, University of California; 1999.
78. Makris N, Kampas G. Size versus slenderness: two competing parameters in the seismic stability of free-standing rocking columns. *Bull Seismol Soc Am*. 2016;106(1):104.
79. Linde SA, Konstantinidis D, Tait MJ. Rocking response of unanchored building contents considering horizontal and vertical excitation. *J Struct Eng (ASCE)*. 2020;146(9):04020175.
80. Lachanas CG, Vamvatsikos D, Vassiliou MF. The influence of the vertical component of ground motion on the probabilistic treatment of the rocking response of free-standing blocks. *Earthq Eng Struct Dyn*. 2022;51(8):1874-1894.

81. Shahi SK, Baker JW. An efficient algorithm to identify strong-velocity pulses in multicomponent ground motions. *Bull Seismol Soc Am*. 2014;104(5):2456-2466.
82. Shahi SK, Baker JW. Pulse classification algorithm. 2012. (Accessed December 2, 2022). <http://www.jackwbaker.com/pulse-classification.html>
83. CESMD, Center for Engineering Strong-Motion Data (CESMD) (Accessed December 2, 2022). <https://www.strongmotioncenter.org/>
84. Goulet CA, Kishida T, Ancheta TD, et al. PEER NGA-east database. *Earthquake Spectra*. 2021;37(1):1331-1353. \_suppl.
85. Boore DM. On pads and filters: processing strong-motion data. *Bull Seismol Soc Am*. 2005;95(2):745-750.
86. Boore DM, Akkar S. Effect of causal and acausal filters on elastic and inelastic response spectra. *Earthq Eng Struct Dyn*. 2003;32(11):1729-1748.
87. Akkar S. Utility Software for Data Processing. (Accessed December 2, 2022). <http://web.boun.edu.tr/sinan.akkar/index.php/usdp/utility-software-for-data-processing>
88. Kazemi H, Khakpour MS. Effect of causality filters of accelerograms on low-rise structure responses. *Pract Period Struct Des Constr*. 2022;27(1):04021053.
89. Trifunac MD. Response spectra of earthquake ground motion. *J Eng Mech Div*. 1978;104(5):1081-1097.
90. Sabetta F, Pugliese A. Estimation of response spectra and simulation of nonstationary earthquake ground motions. *Bull Seismol Soc Am*. 1996;86(2):337-352.
91. Akkar S, Bommer JJ. Influence of long-period filter cut-off on elastic spectral displacements. *Earthq Eng Struct Dyn*. 2006;35(9):1145-1165.
92. Akkar S, Gülkan P, Kale Ö. Uncertainty in nonlinear SDOF response due to long-period noise of accelerograms. *Advances in Performance-Based Earthquake Engineering*. Springer; 2010:69-78.
93. Yim CS, Chopra AK, Penzien J. Rocking response of rigid blocks to earthquakes. *Earthq Eng Struct Dyn*. 1980;8(6):565-587.
94. Riddell R. *Statistical analysis of the response of nonlinear systems subjected to earthquakes*. University of Illinois at Urbana-Champaign; 1979.
95. Sues RH, Wen YK, Ang AHS. Stochastic evaluation of seismic structural performance. *J Struct Eng*. 1985;111(6):1204-1218.
96. Bachmann JA, Strand M, Vassiliou MF, Broccardo M, Stojadinović B. Is rocking motion predictable? *Earthq Eng Struct Dyn*. 2018;47(2):535-552.
97. Vassiliou MF, Broccardo M, Cengiz C, et al. Shake table testing of a rocking podium: results of a blind prediction contest. *Earthq Eng Struct Dyn*. 2021;50(4):1043-1062.
98. Malomo D, Mehrotra A, DeJong MJ. Distinct element modeling of the dynamic response of a rocking podium tested on a shake table. *Earthq Eng Struct Dyn*. 2021;50(5):1469-1475.
99. Zhong C, Christopoulos C. Finite element analysis of the seismic shake-table response of a rocking podium structure. *Earthq Eng Struct Dyn*. 2021;50(4):1223-1230.
100. Del Giudice L, Wróbel R, Katsamakas AA, Leinenbach C, Vassiliou MF. Physical modelling of reinforced concrete at a 1: 40 scale using additively manufactured reinforcement cages. *Earthq Eng Struct Dyn*. 2022;51(3):537-551.
101. Lachanas CG, Vamvatsikos D. Rocking incremental dynamic analysis. *Earthq Eng Struct Dyn*. 2022;51(3):688-703.
102. Lachanas CG, Vamvatsikos D, Dimitrakopoulos EG. Statistical property parameterization of simple rocking block response. *Earthq Eng Struct Dyn*. 2022.
103. Zhong C, Christopoulos C. Scaled shaking table testing of higher-mode effects on the seismic response of tall and slender structures. *Earthq Eng Struct Dyn*. 2022.
104. Psycharis IN, Fragiadakis M, Stefanou I. Seismic reliability assessment of classical columns subjected to near-fault ground motions. *Earthq Eng Struct Dyn*. 2013;42(14):2061-2079.
105. Bakhtiyari E, Gardoni P. Probabilistic seismic demand model and fragility estimates for rocking symmetric blocks. *Eng Struct*. 2016;114:25-34.71.
106. Dimitrakopoulos EG, Paraskeva S. Dimensionless fragility curves for rocking response to near-fault excitations. *Earthq Eng Struct Dyn*. 2015;44(12):2015-2033.
107. Giouvanidis AI, Dimitrakopoulos EG. Rocking amplification and strong-motion duration. *Earthq Eng Struct Dyn*. 2018;47(10):2094-2116.
108. Pappas A, Sextos A, Da Porto F, Modena C. Efficiency of alternative intensity measures for the seismic assessment of monolithic free-standing columns. *Bull Earthquake Eng*. 2017;15(4):1635-1659.
109. Kavvadias IE, Papachatzakis GA, Bantilas KE, Vasiliadis LK, Elenas A. Rocking spectrum intensity measures for seismic assessment of rocking rigid blocks. *Soil Dyn Earthquake Eng*. 2017;101:116-124.
110. Reggiani Manzo N, Lachanas CG, Vassiliou MF, Vamvatsikos D. Uniform risk spectra for rocking structures. *Earthq Eng Struct Dyn*. 2022;51(11):2610-2626.
111. Vassiliou, M. F., & Sieber, M. (2021). Dimensionality reduction of the 3D inverted pendulum cylindrical oscillator and applications on sustainable seismic design of bridges. *Earthquake Engineering & Structural Dynamics*, 51(2), 473–491. Portico. <https://doi.org/10.1002/eqe.3575>
112. Efron B, Tibshirani RJ. An introduction to the bootstrap. 1994: CRC press.

**How to cite this article:** Elmorsy M, Vassiliou MF. Effect of ground motion processing and filtering on the response of rocking structures. *Earthquake Engng Struct Dyn*. 2023;52:1704–1721. <https://doi.org/10.1002/eqe.3837>